Biomaterials Science

In Vitro Model Alveoli From Photodegradable Microsphere Templates

Journal:	*Biomaterials Science*
Manuscript ID:	BM-ART-01-2015-000034.R1
Article Type:	Paper
Date Submitted by the Author:	28-Feb-2015

Complete List of Authors:	Lewis, Katherine; University of Colorado at Boulder, Chemical & Biological Engineering Tibbitt, Mark; University of Colorado at Boulder, Chemical and Biological Engineering; Massachusetts Institute of Technology, David H. Koch Institute for Integrative Cancer Research Zhao, Yi; University of Colorado at Boulder, Chemical and Biological Engineering Branchfield, Kelsey; University of Wisconsin-Madison, Laboratory of Genetics Sun, Xin; University of Wisconsin-Madison, Laboratory of Genetics Balasubramaniam, Vivek; University of Colorado, Pediatric Heart Lung Center Laboratory; University of Wisconsin-Madison, Pediatrics Anseth, Kristi; University of Colorado at Boulder, Chemical and Biological Engineering

Biomaterials Science

RSCPublishing

PAPER

In Vitro Model Alveoli From Photodegradable Microsphere Templates

Cite this: DOI: 10.1039/x0xx00000x

Katherine J. R. Lewis,[a] Mark W. Tibbitt,[a,b] Yi Zhao,[a] Kelsey Branchfield,[c] Xin Sun,[c] Vivek Balasubramaniam[d,e] and Kristi S. Anseth*[a]

Received ooth January 2015,
Accepted ooth January 2015

DOI: 10.1039/x0xx00000x

www.rsc.org/

Recreating the 3D cyst-like architecture of the alveolar epithelium *in vitro* has been challenging to achieve in a controlled fashion with primary lung epithelial cells. Here, we demonstrate model alveoli formed within a tunable synthetic biomaterial platform using photodegradable microspheres as templates to create physiologically relevant, cyst structures. Poly(ethylene glycol) (PEG)-based hydrogels were polymerized in suspension to form microspheres on the order of 120 μm in diameter. The gel chemistry was designed to allow erosion of the microspheres with cytocompatible light doses (≤15 min exposure to 10 mW/cm^2 of 365 nm light) via cleavage of a photolabile nitrobenzyl ether crosslinker. Epithelial cells were incubated with intact microspheres, modified with adhesive peptide sequences to facilitate cellular attachment to and proliferation on the surface. A tumor-derived alveolar epithelial cell line, A549, completely covered the microspheres after only 24 hours, whereas primary mouse alveolar epithelial type II (ATII) cells took ~3 days. The cell-laden microsphere structures were embedded within a second hydrogel formulation at user defined densities; the microsphere templates were subsequently removed with light to render hollow epithelial cysts that were cultured for an additional 6 days. The resulting primary cysts stained positive for cell-cell junction proteins (β-catenin and ZO-1), indicating the formation of a functional epithelial layer. Typically, primary ATII cells differentiated in culture to the alveolar epithelial type I (ATI) phenotype; however, each cyst contained ~1-5 cells that stained positive for an ATII marker (surfactant protein C), which is consistent with ATII cell numbers in native mouse alveoli. This biomaterial-templated alveoli culture system should be useful for future experiments to study lung development and disease progression, and is ideally suited for co-culture experiments where pulmonary fibroblasts or endothelial cells could be presented in the hydrogel surrounding the epithelial cysts.

Introduction

Epithelial cysts are important tissue structures in the body and recent work has employed *in vitro* models to investigate the mechanisms involved in cyst formation and function in many of these tissues, such as the lung,[1–5] mammary glands,[6–9] and kidneys.[10–12] In the lung, hollow epithelial cysts, or alveoli, are clustered at the distal end of bronchioles. Maturation of alveoli occurs postnatally, with secondary septa separating the smooth rudimentary alveoli into many open-sided polyhedra that share a common duct space.[13,14] The major components of alveolar tissue include the single cell layer epithelium attached to the basement membrane and surrounding a hollow central lumen. There are two alveolar epithelial cell phenotypes: ATI cells, which have an elongated morphology, form 95% of the alveolar surface area, and facilitate gas exchange between the lung and the blood stream;[15] and ATII cells, which exhibit a cuboidal morphology, produce lung surfactants, and are the progenitor cells for both the ATII and ATI cell populations in the alveoli.[16]

Many studies concerning alveoli have been focused on understanding alveolar homeostasis[17–20] and the interplay between the epithelium and the mesenchyme during lung development[21–23] and wound healing.[24–28] Much of the *in vitro* work with alveolar epithelial cells has been conducted with 2D monolayers grown on protein-coated stiff substrates such as glass coverslips,[29] tissue culture polystyrene (TCPS),[30] and transwell membranes[31] or seeded on top of soft gels of extracellular matrix (ECM) such as Matrigel[4,26,32] and type I collagen.[33] Nonetheless, 3D tissue structure is critical to normal cellular function,[3,34,35] and therefore, recapitulating the curved cyst architecture is important when designing an *in vitro* alveolar model system. Previously, 3D hollow cysts have been formed from single-cell suspensions of primary alveolar epithelial cells trapped within ECM gels. For example, ATII cells isolated from juvenile rats and embedded within type I collagen gels underwent spontaneous cyst formation over the course of a few weeks in culture.[2] Similarly, adult human ATII cells encapsulated in Matrigel migrated towards each other to

form polarized cysts within 5 days in culture.[1] Unfortunately, spontaneous alveolar cyst formation with primary lung epithelial cells has not been achieved in synthetic hydrogels, where the researcher has a high level of control over matrix properties and biochemical signaling. It should be noted that one example of lung epithelial cells spontaneously forming cysts in a polymer hydrogel has been published,[5] but the authors used a metastatic lung adenocarcinoma cell line, which has significant genetic modifications from a normal, healthy ATII cell. However, with spontaneous *in vitro* formation the final cyst size varies with time in culture, gel composition, and cell seeding density, and reported sizes range from 30 μm to 1 mm, whereas human alveolar size *in vivo* is believed to be on the order of 200 μm in diameter.[36] In order to study the influence of cyst size, matrix mechanics, and matrix signaling on alveolar cell behavior, a user-defined, tunable culture system can be useful to direct cyst formation and manipulate the cyst microenvironment.

Carterson *et al.* employed an interesting technique to create model alveoli by growing A549 cells, a human adenocarcinoma cell line with similarities to the ATII phenotype, on commercial microcarrier beads in suspension culture in a rotating wall vessel reactor.[37] This approach inverts the typical hollow cyst architecture, polarizing the epithelium with the basolateral side facing in to the sphere and the apical side facing out to the medium. While it does allow for facile manipulation of the apical surface, it motivated us to develop a complementary method that would allow one to modify the matrix properties of the adhesive surface and allow for co-culture with cell types found on the basolateral side of the epithelium, such as fibroblasts and endothelial cells.

Synthetic hydrogels, such as those based on a poly(ethylene glycol) (PEG) backbone, exhibit many of the same biophysical qualities as ECM gels (e.g., high water content, tissue-relevant modulus range, as well as facile transport of oxygen and other nutrients) and they are readily modified using several cytocompatible reactions to introduce biochemical signals (i.e., adhesive ligands or growth factors).[38,39] Previous work from our lab has demonstrated the versatility of PEG hydrogels for 3D culture of many primary cell types,[40–43] in particular pioneering the use of the thiol-ene bio-click photoreaction between multi-arm PEGs functionalized with norbornene and cysteine-containing peptides.[44] Using a complementary photocleavage reaction, we also developed a PEG crosslinker that degrades upon exposure to single or two photon light, allowing for softening of the gel or its complete erosion on demand.[45,46] This photodegradable functionality has been incorporated into cell-sized microspheres for drug-delivery applications, allowing the user to completely erode the microspheres with light and release a payload on demand.[47] Building on the microcarrier concept, we aimed to use these photolabile microspheres in a new way, as templates for cyst formation.

Here, we demonstrate the formation and stability of *in vitro* model alveoli using A549 cells or primary ATII cells coated on photodegradable microspheres, serving as sacrificial templates for the hollow cyst tissue structure, and encapsulated in a user-defined hydrogel network. The general procedure is depicted schematically in Figure 1. The diameters of the microspheres were increased to relevant *in vivo* alveolar sizes, and adhesive molecules were incorporated to promote cell attachment to the microspheres. A549 cells or primary ATII cells were incubated with adhesive microspheres to generate cell-coated pre-cysts. The thiol-ene chemistry established by our lab was then used to embed and stabilize these structures in a second hydrogel before erosion of the microsphere templates with cell-compatible light. This process was developed with the A549 cell line, and then expanded to use ATII cells isolated from wild-type mice as an *in vitro* model of healthy alveoli. After template erosion, the cysts maintained their architecture; cells did not infiltrate the central lumen even after 6 days of culture; and they expressed markers of cell junctions and both alveolar epithelial cell phenotypes.

Materials and Methods

Photodegradable Microsphere Synthesis

Photodegradable crosslinker, poly(ethylene glycol) di-photodegradable acrylate (PEGdiPDA; M_n ~ 4070 Da) was synthesized as previously described.[46] Poly(ethylene glycol) tetrathiol (PEG4SH; M_n ~ 5000 Da) was purchased from JenKem Technology USA. Microspheres were formed by inverse suspension polymerization as acrylates on PEGdiPDA underwent a base-catalyzed Michael addition with thiols on PEG4SH in aqueous droplets suspended in an organic phase, as published earlier.[47] Briefly, the organic phase consisted of sorbitan monooleate (Span 80, Sigma-Aldrich) and PEG-sorbitan monooleate (Tween 80, Sigma-Aldrich) in a 3:1 ratio dissolved in hexanes (EMD Millipore), with 30 mg surfactant per mL of hexanes. The aqueous phase was comprised of 6.9 wt% PEGdiPDA, 4.2 wt% PEG4SH, and 300 mM triethanolamine (Sigma-Aldrich) at pH 8.0 in phosphate buffered saline (PBS; Life Technologies), plus the desired adhesive ligand. The adhesive ligands selected here were ultrapure mouse laminin (Corning; 380 nM), fibronectin (BD Biosciences; 450 nM), and CRGDS peptide (American Peptide Company, Inc.; 1.5 mM). The full proteins were entrapped during network formation, whereas the peptide was covalently tethered to the network through the thiol functionality on cysteine. To achieve larger microsphere diameters, the aqueous phase was pipetted into the organic phase and triturated only twice, instead of vortexing the suspension as done previously. In addition, the suspension was stirred at a slower rate (~200 rpm vs. ~600 rpm; Thermolyne Cimarec 2 stir plate with 1 cm magnetic stir bar). Following polymerization, particles were recovered by centrifugation and washed with hexanes, isopropanol, and sterile PBS.

Microsphere Size Characterization

Microspheres were fluorescently tagged with AlexaFluor 488 C_5 maleimide (Life Technologies), which was pre-reacted with the PEG4SH before microsphere synthesis as above. The washed microspheres were diluted in PBS and loaded between a cover slip and a glass slide, separated by a 1 mm rubber gasket. The equilibrium swollen microspheres were then imaged under an epifluorescent microscope (Nikon Eclipse TE2000-S). Images were analyzed using Image J software (NIH). After thresholding the image, microsphere area was measured using the Analyze Particles plug-in. Diameters of 3,087 microspheres were calculated and binned using Excel.

Microsphere Photodegradation

A 0.8 mM solution of PEGdiPDA was prepared in PBS. An absorbance spectrum, 220-748 nm, was taken on a spectrophotometer (NanoDrop 1000; Thermo Scientific) with a path length of 1 mm. This spectrum matches previously published results for the photolabile nitrobenzyl ether (NBE) group.[47] From this spectrum, the molar absorptivity of a NBE group at 365 nm was calculated using Beer's Law, and subsequently used to estimate the

time required to fully erode the microspheres using the equation published by Tibbitt *et al.*[48]:

$$\frac{z_c}{t_c} = \frac{-k_{\text{eff}} I_0}{2.3 \varepsilon_i C_i \ln(1 - P_{\text{rg}})} \quad (1)$$

where z_c is the critical length scale of erosion, t_c is the critical time scale of surface erosion, k_{eff} is the effective kinetic constant of NBE photocleavage, I_0 is the intensity of the incident light, ε_i is the molar absorptivity of the NBE group, C_i is the concentration of the NBE group in the swollen gel, and P_{rg} is the critical fraction of cleaved NBE species, calculated from the Flory-Stockmayer equation.

Particle tracking was used as a method to characterize microsphere photodegradation. Photodegradable microspheres were prepared as above without the adhesive peptide, but containing 2 μm polystyrene beads (FluoSpheres; Life Technologies; 1:100 volume of beads to volume of monomer solution). These microspheres were then encapsulated in thiol-ene PEG gels (described below) and equilibrated in PBS overnight. Bright-field time-lapse images were taken with a confocal microscope (Zeiss LSM 710; every 30 seconds for 15 minutes) before and after exposure of the samples to the 365 nm degrading light at ~10 mW/cm^2 for 15 minutes. MetaMorph software (Molecular Devices) was used to track the beads' positions over time (the solid case had 94 particle trajectories; the liquid case had 74 particle trajectories). These trajectories were corrected for frame drift and an ensemble mean squared displacement was calculated for each time interval using MATLAB. From this plot, an estimate of the particle diffusion coefficient was calculated as previously published, and used to determine the light dose needed to reach the gel to sol transition.[49–51]

Thiol-ene Hydrogel Synthesis

8-arm poly(ethylene glycol) norbornene (PEG-Nb; MW ~40,000 Da) was synthesized as previously described.[44,52] Enzymatically-cleavable di-cysteine peptide (KCGPQG↓IWGQCK) and adhesive peptide (CRGDS) were purchased commercially (American Peptide Company, Inc.). Photoinitiator lithium phenyl-2,4,6-trimethylbenzoylphosphinate (LAP) was synthesized as previously published.[53] To form gel precursor solution, PEG-Nb (10 wt%), peptide crosslinker (0.75 thiol:ene), CRGDS (1 mM), and LAP (0.05 wt%) in sterile PBS were mixed by vortex and the pH was adjusted to 6.8-7.2 by adding sterile-filtered 0.1 M sodium hydroxide. Pre-cysts or single-cell suspensions were added to this gel precursor solution and gently mixed with a pipette. Gels were formed by placing 30 μL of gel precursor solution onto a Sigmacote-treated glass slide, positioning a 1 mm thick rubber gasket around the droplet, and covering it with a second Sigmacote-treated glass slide. This mold was then exposed to 365 nm light at ~10 mW/cm^2 for 3 min to initiate the radical-mediated thiol-ene step-growth polymerization reaction. After gelation, the glass slides were separated and the free gel was transferred to an untreated 24-well plate with 1 mL appropriate growth medium. Gels were kept at 37 °C with 5% CO_2 for 1 day before microsphere template erosion.

A549 Cell Culture

A549 human adenocarcinoma cells (ATCC, CCL-185) were cultured in standard growth medium (Dulbecco's modified Eagle's medium (DMEM), 10% fetal bovine serum (FBS), 2% penicillin/streptomycin (100 U/mL), 0.4% fungizone (0.5 μg/mL), Invitrogen) at 37 °C with 5% CO_2 and passaged until use in experiments. For viability experiments, cells were trypsinized, centrifuged, and resuspended at 25 million cells/mL in PBS. For seeding on microspheres, cells were trypsinized, centrifuged, and resuspended at 1 million cells/mL in growth medium.

Viability Experiments

A549 cells were encapsulated at 6.7 million cells/mL in thiol-ene gels as described above. The day after encapsulation, half the gels were exposed to 365 nm light at ~10 mW/cm^2 for 15 min, and half remained in the dark. A Live/Dead cell viability assay (Life Technologies) was performed an hour later, and one day later. Gels were immediately imaged on a confocal microscope (Zeiss LSM 710), and image stacks were analyzed for red cell count (dead) and green cell count (live) with MATLAB.

ATII Isolation and Culture

All procedures and protocols were reviewed and approved by the Animal Care and Use Committee at the University of Colorado Denver Anschutz Medical Campus. Mice were obtained from The Jackson Laboratories and bred in-house.

Primary ATII cells were isolated from FVB/NJ mice (6-8 weeks old) as previously described.[42] Briefly, mice were euthanized by CO_2 asphyxiation, the chest was opened, and sterile saline was injected into right ventricle to clear the blood from the pulmonary circulation. The heart lung block was then excised and distal lung tissue was trimmed away from the heart, trachea and other tissue and finely minced. Lung tissue was digested in 1% collagenase (Worthington Biochemical) and 1 mg/mL DNase (Sigma) for 20 minutes at 37 °C. Then, trypsin (Fisher) was added (final concentration of 0.01%) and incubated for 20 minutes. Next, a solution of 1 mg/mL trypsin inhibitor and 1 mg/mL DNase was added and the mixture was passed through a 100 μm cell strainer to remove large undigested lung sections, followed by filtration through a Nitex Filter (10 μm pore diameter). The filtered lung solution was centrifuged for 8 min at 480 *g*, and the cell pellet was washed with DMEM/F12 media. Immune cells were separated from epithelial cells by adding the cell suspension to tissue culture plates coated with IgG (11 mg/cm^2) and incubating for 1 hour at 37 °C. Non-adherent cells were recovered and centrifuged at 480 *g* for 8 min. Cells were resuspended at 1 million cells/mL in growth medium supplemented with hepatocyte growth factor (HGF; R&D Systems; 50 ng/mL) and keratinocyte growth factor (KGF; Sigma; 10 ng/mL) prior to using in cyst experiments.

Cell-Microsphere Seeding

To seed photodegradable microspheres with cells, either A549 cells at 200,000 cells/mL or ATII cells at 500,000 cells/mL were placed in an ultra-low adhesion 24-well plate (Corning) with 40 μL microspheres in sterile PBS. The plate was placed on an orbital shaker at 45 rpm and incubated at 37 °C with 5% CO_2 overnight. A549 cells were incubated for 1 day to enable full coating of the microspheres, whereas ATII cells were incubated for 3 days before encapsulation in hydrogels. These cell-microsphere structures are referred to here as pre-cysts. Brightfield images of cell seeding were taken on an inverted epifluorescent microscope (Nikon Eclipse TE2000-S).

Template Erosion

Cell-laden microspheres were encapsulated in thiol-ene gels and cultured for one day to enable formation of cellular attachments to the encapsulating gel. Gels were exposed to 365 nm light at ~10 mW/cm^2 for 15 minutes to cleave the photodegradable moiety and completely erode the microsphere templates. The low molecular weight degradation products were allowed to swell out of the gels for 1 hour before the media was changed. Thereafter, media was changed daily, with the growth factor-supplemented media prepared fresh every other day for the primary cysts. Cysts were typically cultured for another 3-6 days after template erosion.

Immunostaining and Imaging

At the completion of each experiment, samples were fixed in 4% paraformaldehyde in PBS for 15 minutes at room temperature and washed 3 times with PBS. Cells were subsequently permeabilized in 1% TritonX-100, and samples were blocked overnight with 40% goat serum in PBS. Primary antibodies used in these experiments were rabbit anti-prosurfactant protein C (SPC; 1:100; Millipore), hamster anti-mouse podoplanin (T1α; 1:100; eBioscience), mouse anti-β-catenin (1:100; Invitrogen), and rabbit anti-ZO-1 (1:100; Invitrogen). Secondary antibodies used in these experiments were goat anti-rabbit AlexaFluor 594 (1:200; Life Technologies), goat anti-hamster AlexaFluor 488 (1:200; Life Technologies), and goat anti-mouse AlexaFluor 488 (1:200; Life Technologies). For the whole mount gels, samples were incubated with primary antibodies overnight at 4 °C, followed by 3 wash steps (twice for 1 hour, and once overnight). Samples were then incubated with secondary antibodies overnight at 4 °C, followed by 3 wash steps (twice for 1 hour, and once overnight). Finally, nuclei were stained with DAPI (1:2000; Invitrogen) for 1 hour at room temperature, and samples were washed twice for 30 minutes and once overnight in PBS.

In one experiment, A549 cysts were fixed and permeabilized as before, followed by staining with DAPI (1:2000; Invitrogen) and TRITC-Phalloidin (1:200; Sigma) for 1 hour at room temperature to label the nuclei and actin cytoskeleton.

All samples were imaged on a confocal microscope (Zeiss LSM 710) with a 20x water-dipping objective (Plan Appochromat; NA=1.0). Image stacks were taken from the top of a cyst to the bottom (z step = 5 μm), and analyzed in ImageJ software (NIH).

Histological Sectioning of Cysts

To verify that the cysts' central lumen remained free of cells after template erosion, one set of primary cysts in gels was fixed as before and then prepared for cryosectioning. Gels were swollen in HistoPrep (Fisher) overnight at 4 °C, then flash frozen in liquid nitrogen for ~10 seconds. These were transferred to molds containing room temperature HistoPrep and covered with a small drop of HistoPrep. The molds were then flash frozen in liquid nitrogen and slowly warmed to -22 °C in a cryostat (Leica CM1850). 50 μm sections were cut and mounted onto microscope slides. These sections were then stained as before for T1α, SPC, and DAPI, and imaged on a confocal microscope (Zeiss LSM 710).

Histological Sectioning of Mouse Lungs

Mouse lungs were fix inflated with 4% paraformaldehyde. Tissue sections of 75 μm thickness were prepared using a vibratome. Sections were stained with the following antibodies: rabbit anti-SPC (1:200; Seven Hills Bioreagents), Syrian hamster anti-T1alpha (1:100; Developmental Studies Hybridoma Bank) and goat anti-rabbit Cy3 or goat anti-syrian hamster FITC (1:200; Jackson ImmunoResearch Laboratories).

Labeled cells were observed with a confocal laser scanning microscope LSM 510 (Carl Zeiss, Germany) equipped with an argon laser (excitation 488 nm) and a DPS laser (excitation 561 nm). Serial optical sections were captured over a total depth of 50 um with a 0.5 um z-step. Three-dimensional reconstructions and rotating movies were generated using IMARIS analysis software (Bitplane, Switzerland). Three-dimensional surface projections were shown for visualization of lung architecture.

Results and Discussion

Alveoli in the native lung are roughly spherical, with an approximate diameter of 200 μm in human lungs.[36] The alveolar epithelium consists of flattened ATI cells interspersed with rounded ATII cells, typically found where neighboring alveoli meet.[54] To maintain a barrier between the airway and the vasculature, these epithelial cells form tight junctions and adherens junctions, as evidenced by expression of ZO-1 and β–catenin, respectively. To model this spherical epithelial arrangement *in vitro,* we developed a templating procedure with hydrogels, exploiting the photochemistry previously developed in our laboratory to create sacrificial spherical molds for the epithelial cells to adhere to. The general procedure is to form bioadhesive photodegradable microspheres, seed these microspheres with epithelial cells, encapsulate the cell-microsphere structures (referred to from here on as pre-cysts) inside a second hydrogel, and erode the microsphere template with light, leaving a hollow epithelial cyst attached to the surrounding hydrogel (Figure 1).

Microsphere Synthesis and Characterization

The microsphere template consisted of an 11.1 wt% PEG macromer solution formed as aqueous droplets suspended in an organic phase to make spherical particles. The polymer network was formed via spontaneous base-catalyzed Michael addition between the thiol groups on PEG4SH and the acrylate groups on PEGdiPDA (Fig. 2A). A small, commonly used peptide (CRGDS; Fig. 2A) that binds to integrin receptors on the cell surface was covalently tethered to the polymer network through the thiol group on the n-terminal cysteine. Many types of adhesive ligands could be included in these microspheres, and early work with A549 cells presented here used full proteins (laminin or fibronectin) physically entrapped in the gel network during polymerization. Proteins larger than ~25 kDa are readily entrapped in the network and other thiol-containing peptides or thiolated proteins can be reacted into the polymer network, as desired.

A maleimide-conjugated AlexaFluor 488 dye was reacted into the microsphere network to measure the size distribution of the microspheres by image analysis (Fig. 2B; n = 3087 particles). The microspheres had an average diameter of 120 ± 70 μm with a polydispersity of 1.4, and 90% of the particles were <200 μm in diameter. This size range is relevant to mammalian alveoli *in vivo,* with human alveoli diameters on the order of 200 μm and mouse alveoli diameters on the order of 50 μm.[55]

The nitrobenzyl ether (NBE) groups in the PEGdiPDA crosslinker (yellow in Fig. 2A) are susceptible to cleavage by light, as depicted in Fig. 2C. The absorbance spectrum (Fig. 2C) of the crosslinker shows that the NBE moieties strongly absorb light between 300-400 nm, as has been previously reported.[45–47] Light at 365 nm was chosen for erosion of the microspheres because it has been shown many times to be cytocompatible and light sources are readily available. Beer's Law was used to calculate the molar absorptivity of the NBE moiety at 365 nm (ε_{365} = 5,000 L mol^{-1} cm^{-1}). Since the microspheres are optically thick (A > 0.1), erosion is limited to the top surface of the gel until the degradation products diffuse out of the light path and allow more light to reach deeper sections of the gel. Using the models published by Tibbitt *et al.,* a rate at which erosion progresses through the microspheres can be calculated with Equation 1.[48] Briefly, this rate depends on the effective rate of photocleavage of the NBE group, the intensity of the incident light, the molar absorptivity of the NBE group, the concentration of NBE in the gel, and the critical fraction of cleaved NBE groups to reach reverse gelation. For this step growth network, reverse gelation occurs when 42% of the crosslinks have been cleaved. Using the calculated erosion rate (13.5 μm/min with 365 nm light at 10

mW/cm^2), we estimated that a 100 μm diameter microsphere would take 7.4 minutes to fully erode and a 200 μm diameter microsphere would take 15 minutes to fully erode.

To confirm these estimates and directly measure erosion, we characterized the gel to sol transition by entrapping 2 μm beads inside the hydrogel microspheres, encapsulating them inside thiol-ene hydrogels, and using time-lapse microscopy to look for Brownian motion of the beads (Fig. 2D). Before erosion of the microspheres, but after experiencing the 3-minute thiol-ene gel polymerization with 365 nm light, the beads were stationary, indicating the microspheres were still solid gels. After exposure to another 15 minutes of 365 nm light at ~10 mW/cm^2, the beads moved randomly through the space where the microsphere had been, indicating the microsphere had eroded to a liquid. By tracking bead position over time, the ensemble mean squared displacement curve was calculated for 94 beads in the solid case and 74 beads in the liquid case. From this plot, the diffusion coefficient was estimated to be 0.050 μm^2/min for the solid case and 0.94 μm^2/min for the liquid case. This corresponds to a viscosity of 0.13 Pa•s for the solid case and 0.0069 Pa•s for the liquid case. Since the eroded microspheres had a viscosity that is two orders of magnitude lower than that of the microspheres before exposure to light, we conclude that the gel network is completely degraded and no solid gel or surface remains to promote cell attachment. Further evidence that the microsphere network erodes with this light dose came from the observation that A549 cell layers attached to microspheres would swell as polymer crosslinks were cleaved and then collapse when the network reached reverse gelation (ESI Video 1). Encapsulation in a second hydrogel was necessary to stabilize the cysts during and after template erosion (ESI Video 2).

Encapsulation of Lung Epithelial Cells in Thiol-Ene Hydrogels

Before encapsulating pre-cyst structures in the thiol-ene gels, the compatibility of the gel for permitting high survival of single cells was studied. The encapsulating hydrogel consisted of a norbornene-functionalized 8-arm PEG and a di-cysteine peptide crosslinker (KCGPQG↓IWGQCK) derived from a sequence known to be cleavable by cell-secreted matrix metalloproteinases (Fig. 3A).[56] The norbornene and thiol groups undergo photoinitiated radical polymerization to form a step-growth network.[44] Again, the adhesive peptide CRGDS was covalently bound to the network through the thiol on the cysteine. Here, too, the adhesive ligand can be varied easily with different cysteine-containing peptides, if desired. While not shown in this work, the elastic modulus of the encapsulating gel is also tunable by varying the weight percent of the PEG macromer or by changing the stoichiometric ratio of the thiol groups on the peptide crosslinker to the ene groups on the PEG.[41,43,52,57] For the specific formulation studied here, the elastic modulus was ~20 kPa, which is within the reported range of moduli for healthy lung tissue (*i.e.*, 5-30 kPa).[58,59]

This hydrogel system was shown to be cytocompatible by encapsulating a single-cell suspension of A549 cells, staining for the actin cytoskeleton to show typical rounded cell morphology (Fig. 3B), and performing a cell viability assay (Fig. 3C). Cell survival was high with 93 ± 3% cells staining positive with the live marker one day after encapsulation. To further probe cell viability during the cyst-making process, encapsulated A549 cells were exposed to 15 minutes of 365 nm light at ~10 mW/cm^2, the same light dose used to erode the microsphere templates. Viability one hour and one day after light exposure were both 90 ± 4% live, which is not statistically different from the cells left in the dark.

Testing the Procedure with A549 Cells

Cyst-like structures were formed using the characterized, photodegradable microspheres and the cytocompatible, thiol-ene hydrogels. During the cyst-forming process, the cells experience three distinct matrix situations (Fig. 4). First, the cells attach to the RGD in the microsphere template and spread and proliferate to form a complete epithelial layer on the carrier hydrogel. Next, the pre-cysts are encapsulated in the thiol-ene hydrogel and the cells form additional attachments to the RGD in the second gel. Finally, the microsphere templates are eroded, leaving only the encapsulating gel for the cells to adhere to and a hollow central lumen where the microsphere had been. While polymer degradation products including CRGDS peptides are initially present after template erosion, fast integrin turnover and diffusion of small-molecule products through gaps in the epithelium contribute to the lack of ECM signaling inside the cyst lumen in the hours and days following erosion.

First, the A549 cell line was employed to test the cyst templating procedure, because of its ease of culture, rapid proliferation, and previous use in the literature as a model cell line for the ATII phenotype.[28,37,60] To coat the microsphere templates with cells, A549s and fibronectin-loaded microspheres were combined in an ultra-low adhesion 24-well plate and incubated on an orbital shaker. The wells were monitored by bright field microscopy, and cells were shown to completely cover the microspheres within 24 hours (Fig. 5A). Interestingly, this coating time did not significantly change with several different adhesive proteins (laminin, fibronectin) or peptide adhesive ligands (RGD) that were examined (data not shown). After 24 hours of coating, the pre-cysts were encapsulated in the thiol-ene gel as described above and allowed to form attachments to this new substrate for another 24 hours. Next, the microsphere template was eroded with 365 nm light at ~10 mW/cm^2 for 15 minutes (Fig. 5B,C), as determined earlier. The cysts were cultured three more days after template erosion before being fixed and stained for the actin cytoskeleton and the cell nucleus (Fig. 5D,E). The A549 cysts remained roughly spherical in culture, and the confocal slice demonstrates that the central lumen remained free of cells after erosion of the microsphere template. The A549 cell line is limited in its use due to the rapid proliferation of this adenocarcinoma cell line and the lack of appropriate apical-basal polarity. Cysts formed utilizing this cell line have multiple cell layers and display rough edges, which is atypical of a healthy alveolus. However, the A549 cysts may be useful in studying cancer progression of the alveolar epithelium.

Primary Alveolar Epithelial Cell Cysts

ATII cells isolated from healthy mice were used in the same cyst templating procedure described above. In contrast with the highly proliferative A549 cell line, these primary cells took three days to spread and cover the microspheres completely (Fig. 6A). As before, the pre-cysts were encapsulated and the microsphere templates were eroded one day after encapsulation (Fig. 6B). The cysts were cultured another 3-6 days (7-10 days after isolation from the mice) and fixed and stained for cell phenotype markers (Fig. 6C,D). The primary cysts also remained spherical with empty central lumens. To confirm that no cells infiltrated the lumen and prove that imaging with the confocal microscope does not suffer from complete light

attenuation in the center of these cysts, gels containing primary cysts were cryosectioned into 50 μm sections and stained and imaged as before (Fig. 6E). Sections of one half of a cyst are presented here to demonstrate that the cyst interior remained devoid of cells. The primary cysts were noticeably smoother than the A549 cysts and displayed an epithelium that was typically only one or two cells thick, which is more in keeping with the native alveolar architecture. Primary cysts had an average diameter of 180 ± 80 μm, which is in the size range relevant to human alveoli (~200 μm). The average cyst diameter was larger than that of the original microspheres, but that may have been caused by sampling bias when selecting cysts to image, or the smaller pre-cysts may have preferentially adhered to the well plate and been left behind when the pre-cysts were transferred to the gel precursor solution. One intriguing possibility for the increased luminal volume is that ATII cells may have secreted surfactant lipids and proteins into the central lumen, although we have not yet explored this option.

Hallmarks of any epithelial layer are the formation of adherens junctions to connect the cytoskeletons of neighboring cells and tight junctions between the cells to provide a barrier against passive solute diffusion. To further characterize the primary cysts, we stained for the cell junction proteins β-catenin (adherens junctions) and ZO-1 (tight junctions) (Fig. 7A,B). β-catenin was bright along the cell membranes throughout the cyst, indicating mature adherens junction formation between these epithelial cells. ZO-1 was less widely distributed, but it did appear in many of the cells, demonstrating at least partial formation of tight junctions in the cyst. Further development of these junctions may require more time in culture.

Finally, primary cysts were stained and analyzed for cell phenotype (Fig. 7C,D). Surfactant protein C (SPC) is produced by ATII cells and stored in the cell cytosol and is commonly used as a marker of ATII cell phenotype. T1α is located in the cell membrane of ATI cells and is a marker of the ATI cell phenotype. As is typically seen in culture *in vitro,*[30,61] the freshly isolated ATII cells quickly differentiated on the microspheres into ATI-like cells with an elongated morphology, positive staining for T1α, and almost no staining for SPC. The number of cells per cyst positive for SPC was very small (3 ± 2 per cyst). However, this number may be relevant to native alveoli, because the 3D surface reconstruction of a 50-micron section of mouse lung tissue shown in Figure 7E suggests that each mouse alveolus only contains 1 or 2 ATII cells (to view this reconstruction from multiple angles see ESI Video 3). When compared to the mouse cysts in the lung tissue section, the engineered cysts recreate the approximate size scale and small numbers of ATII cells, although the total number of cells in the engineered cysts is much higher. Collectively, the evidence presented indicates that the epithelial cysts developed here capture many aspects of the structure and cellular arrangement found in alveoli *in vivo,* and may be useful as *in vitro* models of the distal airway epithelium for future experiments.

Conclusions

We have developed an *in vitro* 3D model of the alveolar epithelium using photodegradable microspheres as sacrificial templates to form spherical multi-cellular structures with hollow interiors, cultured within a tunable hydrogel scaffold. This procedure was demonstrated with a tumor-derived alveolar epithelial cell line as well as primary mouse ATII cells, the majority of which differentiated into ATI-like cells. Given the size range, cellular arrangement, cell junction protein and phenotype marker expression demonstrated here, these model alveoli captured several of the same biological aspects of alveoli *in vivo*. Recapitulating the native alveolar tissue architecture within an easily modifiable synthetic platform provides an avenue for numerous experiments previously unattainable *in vitro*. For instance, bulk matrix properties can be systematically varied to determine their influence on cell phenotype or cellular response to external signals such as inflammatory cytokines. Moreover, this model is particularly suited for co-culture experiments with epithelial cysts surrounded by a second cell type such as pulmonary fibroblasts or endothelial cells, both of which play key roles during lung development and disease progression. We believe that this cyst model will be a valuable tool for those studying the biology of the lung epithelium, as well as screening potential therapeutics for treating diseases, such as lung fibrosis.

Acknowledgements

The authors would like to thank Emi Kiyotake for histological sectioning, particle tracking, and image analysis and Sharon Ryan for mouse cell isolations. This work was supported in part by a grant from the National Science Foundation (CTS1236662) and the Howard Hughes Medical Institute.

Notes and references

[a] Department of Chemical and Biological Engineering, the BioFrontiers Institute, and the Howard Hughes Medical Institute, University of Colorado at Boulder, 3415 Colorado Ave, 596 UCB, Boulder, CO 80303, USA. E-mail: kristi.anseth@colorado.edu; Fax: +1-303-492-4341; Tel: +1-303-735-5336

[b] Current address: David H. Koch Institute for Integrative Cancer Research, Massachusetts Institute of Technology, Cambridge, MA 02139, USA.

[c] Laboratory of Genetics, University of Wisconsin-Madison, Madison, WI 53706, USA.

[d] Pediatric Heart Lung Center Laboratory, University of Colorado, Denver, CO, USA.

[e] Current address: Department of Pediatrics, University of Wisconsin-Madison, 600 Highland Avenue, K4/922, Madison, WI 53792, USA.

Electronic Supplementary Information (ESI) available. See DOI: 10.1039/b000000x/

References

1. W. Yu, X. Fang, A. Ewald, K. Wong, C. A. Hunt, Z. Werb, M. A. Matthay, and K. Mostov, *Mol. Biol. Cell*, 2007, **18**, 1693.

2. H. Sugihara, S. Toda, S. Miyabara, C. Fujiyama, and N. Yonemitsu, *Am. J. Pathol.*, 1993, **142**, 783–92.

3. M. J. Mondrinos, S. Koutzaki, E. Jiwanmall, M. Li, J.-P. Dechadarevian, P. I. Lelkes, and C. M. Finck, *Tissue Eng.*, 2006, **12**, 717–28.

4. M. L. Matter and G. W. Laurie, *J. Cell Biol.*, 1994, **124**, 1083–90.

5. B. J. Gill, D. L. Gibbons, L. C. Roudsari, J. E. Saik, Z. H. Rizvi, J. D. Roybal, J. M. Kurie, and J. L. West, *Cancer Res.*, 2012, **72**, 6013–23.

6. J. A. Sharp, K. N. Cane, S. L. Mailer, W. H. Oosthuizen, J. P. Y. Arnould, and K. R. Nicholas, *Matrix Biol.*, 2006, **25**, 430–42.

7. R. Montesano and P. Soulié, *J. Cell Sci.*, 2002, **115**, 4419–4431.

8. M. J. Paszek, N. Zahir, K. R. Johnson, J. N. Lakins, G. I. Rozenberg, A. Gefen, C. A. Reinhart-King, S. S. Margulies, M. Dembo, D. Boettiger, D. A. Hammer, and V. M. Weaver, *Cancer Cell*, 2005, **8**, 241–54.

9. M. J. Bissell, A. Rizki, and I. S. Mian, *Curr. Opin. Cell Biol.*, 2003, **15**, 753–762.

10. K. M. Schumacher, S. C. Phua, A. Schumacher, and J. Y. Ying, *Kidney Int.*, 2008, **73**, 1187–92.

11. F. Martín-Belmonte, W. Yu, A. E. Rodríguez-Fraticelli, A. Ewald, Z. Werb, M. A. Alonso, and K. Mostov, *Curr. Biol.*, 2008, **18**, 507–13.

12. L. O'Brien, M. Zegers, and K. Mostov, *Nat. Rev. Mol. Cell*, 2002, **3**, 531–537.

13. P. H. Burri, *Biol. Neonate*, 2006, **89**, 313–322.

14. H. Kitaoka, G. F. Nieman, Y. Fujino, D. Carney, J. DiRocco, and I. Kawase, *J. Physiol. Sci.*, 2007, **57**, 175–185.

15. M. C. Williams, *Annu. Rev. Physiol.*, 2003, **65**, 669–95.

16. R. J. Mason, *Respirology*, 2006, **11**, S12–S15.

17. L. Guillot, N. Nathan, O. Tabary, G. Thouvenin, P. Le Rouzic, H. Corvol, S. Amselem, and A. Clement, *Int. J. Biochem. Cell Biol.*, 2013, **45**, 2568–73.

18. B. D. Uhal, *Am. J. Physiol. Cell. Mol. Physiol.*, 1997, **272**, L1031–1045.

19. B. L. M. Hogan, C. E. Barkauskas, H. A. Chapman, J. A. Epstein, R. Jain, C. C. W. Hsia, L. Niklason, E. Calle, A. Le, S. H. Randell, J. Rock, M. Snitow, M. Krummel, B. R. Stripp, T. Vu, E. S. White, J. A. Whitsett, and E. E. Morrisey, *Cell Stem Cell*, 2014, **15**, 123–38.

20. C. Barkauskas, M. Cronce, C. Rackley, E. Bowie, D. Keene, B. Stripp, S. Randell, P. Noble, and B. Hogan, *J. Clin. Invest.*, 2013, **123**, 3025–3036.

21. W. Y. Park, B. Miranda, D. Lebeche, G. Hashimoto, and W. V Cardoso, *Dev. Biol.*, 1998, **201**, 125–34.

22. S. Bellusci, J. Grindley, H. Emoto, N. Itoh, and B. L. Hogan, *Development*, 1997, **124**, 4867–78.

23. N. Tang, W. F. Marshall, M. McMahon, R. J. Metzger, and G. R. Martin, *Science*, 2011, **333**, 342–345.

24. A.-K. T. Perl and E. Gale, *Am. J. Physiol. Lung Cell. Mol. Physiol.*, 2009, **297**, L299–308.

25. T. Yano, R. J. Mason, T. Pan, R. R. Deterding, L. D. Nielsen, and J. M. Shannon, *Am. J. Physiol. Lung Cell. Mol. Physiol.*, 2000, **279**, L1146–58.

26. K. Sugahara, J. Tokumine, K. Teruya, and T. Oshiro, *Respirology*, 2006, **11**, S28–31.

27. L. M. Crosby and C. M. Waters, *Am. J. Physiol. Lung Cell. Mol. Physiol.*, 2010, **298**, 715–731.

28. S. Prasad, C. M. Hogaboam, and G. Jarai, *Fibrogenesis Tissue Repair*, 2014, **7**, 7.

29. B. E. Isakson, G. J. Seedorf, R. L. Lubman, and S. Boitano, *In Vitro Cell. Dev. Biol. Anim.*, 2002, **38**, 443–9.

30. M. Bhaskaran, N. Kolliputi, Y. Wang, D. Gou, N. R. Chintagari, L. Liu, and T. G. F. Signaling, *J. Biol. Chem.*, 2007, **282**, 3968 –3976.

31. R. Qiao, W. Yan, C. Clavijo, R. Mehrian-Shai, Q. Zhong, K.-J. Kim, D. Ann, E. D. Crandall, and Z. Borok, *Am. J. Respir. Cell Mol. Biol.*, 2008, **38**, 239–46.

32. J. Wang, K. Edeen, R. Manzer, Y. Chang, S. Wang, X. Chen, C. J. Funk, G. P. Cosgrove, X. Fang, and R. J. Mason, *Am. J. Respir. Cell Mol. Biol.*, 2007, **36**, 661–8.

33. T. Umino, H. Wang, Y. Zhu, X. Liu, L. S. Manouilova, J. R. Spurzem, M. P. Leuschen, and S. I. Rennard, *Am. J. Respir. Cell Mol. Biol.*, 2000, **22**, 702–707.

34. M. J. Bissell, P. A. Kenny, and D. C. Radisky, *Cold Spring Harb. Symp. Quant. Biol.*, 2005, **70**, 343–56.

35. L. G. Griffith and M. A. Swartz, *Nat. Rev. Mol. Cell Biol.*, 2006, **7**, 211–24.

36. M. Ochs, J. R. Nyengaard, A. Jung, L. Knudsen, M. Voigt, T. Wahlers, J. Richter, and H. J. G. Gundersen, *Am. J. Respir. Crit. Care Med.*, 2004, **169**, 120–4.

37. A. Carterson, K. zu Bentrup, C. Ott, M. Clarke, D. Pierson, C. Vanderburg, K. Buchanan, C. Nickerson, and M. Schurr, *Infect. Immun.*, 2005, **73**, 1129–1140.

38. M. W. Tibbitt and K. S. Anseth, *Biotechnol. Bioeng.*, 2009, **103**, 655–63.

39. K. J. R. Lewis and K. S. Anseth, *MRS Bull.*, 2013, **38**, 260–268.

40. C. N. Salinas and K. S. Anseth, *Biomaterials*, 2008, **29**, 2370–7.

41. J. A. Benton, B. D. Fairbanks, and K. S. Anseth, *Biomaterials*, 2009, **30**, 6593–603.

42. A. M. Kloxin, K. J. R. Lewis, C. A. Deforest, G. Seedorf, M. W. Tibbitt, V. Balasubramaniam, and K. S. Anseth, *Integr. Biol.*, 2012, **4**, 1540–1549.

43. D. D. McKinnon, A. M. Kloxin, and K. S. Anseth, *Biomater. Sci.*, 2013, **1**, 460.

44. B. D. Fairbanks, M. P. Schwartz, A. E. Halevi, C. R. Nuttelman, C. N. Bowman, and K. S. Anseth, *Adv. Mater.*, 2009, **21**, 5005–5010.

45. A. M. Kloxin, A. M. Kasko, C. N. Salinas, and K. S. Anseth, *Science*, 2009, **324**, 59–63.

46. A. M. Kloxin, M. W. Tibbitt, and K. S. Anseth, *Nat. Protoc.*, 2010, **5**, 1867–87.

47. M. W. Tibbitt, B. W. Han, A. M. Kloxin, and K. S. Anseth, *J. Biomed. Mater. Res. Part A*, 2012, **100A**, 1647–1654.

48. M. Tibbitt, A. Kloxin, L. Sawicki, and K. Anseth, *Macromolecules*, 2013, **46**, 2785–2792.

49. X. Michalet, *Phys. Rev. E*, 2010, **82**, 041914.

50. D. Ernst and J. Köhler, *Phys. Chem. Chem. Phys.*, 2013, **15**, 845–9.

51. R. Shenoy, M. W. Tibbitt, K. S. Anseth, and C. N. Bowman, *Chem. Mater.*, 2013, **25**, 761–767.

52. S. T. Gould, N. J. Darling, and K. S. Anseth, *Acta Biomater.*, 2012, **8**, 3201–9.

53. B. D. Fairbanks, M. P. Schwartz, C. N. Bowman, and K. S. Anseth, *Biomaterials*, 2009, **30**, 6702–7.

54. E. L. Herzog, A. R. Brody, T. V Colby, R. Mason, and M. C. Williams, *Proc. Am. Thorac. Soc.*, 2008, **5**, 778–82.

55. S. E. Soutiere, C. G. Tankersley, and W. Mitzner, *Respir. Physiol. Neurobiol.*, 2004, **140**, 283–91.

56. M. P. Lutolf, J. L. Lauer-Fields, H. G. Schmoekel, A. T. Metters, F. E. Weber, G. B. Fields, and J. A. Hubbell, *Proc. Natl. Acad. Sci. U. S. A.*, 2003, **100**, 5413–8.

57. K. A. Kyburz and K. S. Anseth, *Acta Biomater.*, 2013, **9**, 6381–92.

58. F. S. A. Cavalcante, S. Ito, K. Brewer, H. Sakai, A. M. Alencar, M. P. Almeida, J. S. Andrade, A. Majumdar, E. P. Ingenito, and B. Suki, *J. Appl. Physiol.*, 2005, **98**, 672–9.

59. I. Levental, P. C. Georges, and P. A. Janmey, *Soft Matter*, 2007, **3**, 299–306.

60. K. A. Foster, C. G. Oster, M. M. Mayer, M. L. Avery, and K. L. Audus, *Exp. Cell Res.*, 1998, **243**, 359–66.

61. B. Isakson, R. Lubman, G. Seedorf, and S. Boitano, *Am J Physiol Cell Physiol*, 2001, **281**, C1291–C1299.

Fig. 1 Schematic of the overall cyst-forming procedure, cross-sectional view. (i) Bioadhesive, photodegradable microspheres (orange) were (ii) incubated with epithelial cells (purple) to coat the surface of the microspheres with cells. The cell-microsphere pre-cyst structures were (iii) encapsulated in a second bioadhesive hydrogel (blue), followed by (iv) erosion of the microsphere template with 365 nm light, leaving a hollow epithelial cyst inside the encapsulating hydrogel.

Fig. 2 Microsphere synthesis and erosion. (A) The microsphere hydrogel network was composed of poly(ethylene glycol) tetrathiol (PEG4SH; M_n ~5 kDa) and poly(ethylene glycol) di-photodegradable acrylate (PEGdiPDA; Mn ~4.1 kDa), with the bioadhesive peptide CRGDS included at 1.5 mM. The monomers were reacted via an inverse suspension polymerization using a base-catalyzed Michael addition to form the microspheres. (B) Microspheres labeled with a green fluorescent dye were imaged and analyzed to determine the size distribution. Histogram shows distribution of microsphere diameters, and the black line indicates the cumulative percentage of the population. Inset shows representative fluorescent image of microspheres used for diameter measurement. n = 3087 (C) The chemical structure indicates the cleavage of the nitrobenzyl ether moiety with light. The absorbance spectrum is for the PEGdiPDA crosslinker (0.8 mM) in phosphate-buffered saline, where the blue line indicates 365 nm. The molar extinction coefficient at 365 nm for the nitrobenzyl ether moiety was calculated to be ~5,000 L mol^{-1} cm^{-1}. (D) Microspheres containing entrapped 2 μm diameter polystyrene beads were encapsulated in a second hydrogel and exposed to 365 nm light at an intensity of ~10 mW/cm^2 for 15 minutes to erode the microspheres. Images are of polystyrene bead tracks over 15 minutes before and after light exposure illustrating increased Brownian motion after microsphere erosion. The plot gives the ensemble mean squared displacement for the liquid and solid cases.

Fig. 3 Encapsulating hydrogel formulation. (A) The encapsulating gel was composed of 8-arm poly(ethylene glycol) functionalized with norbornene end groups (M_n ~40 kDa) and an enzymatically-cleavable di-cysteine peptide crosslinker (KCGPQG↓IWGQCK), with the adhesive peptide CRGDS included at 1 mM. The arrow indicates the enzymatic cleavage site. Thiol groups (red) react with the -ene functionalities on the 8-arm PEG through a radical-initiated thiol-ene polymerization. (B) Single cell suspension of A549 cells encapsulated in the thiol-ene gel. The image is a z-projection of a 250 μm confocal stack showing healthy actin cytoskeleton (red) and cell nuclei (blue). (C) Single cell suspension of A549 cells encapsulated in thiol-ene gels. The images are z-projections of a 500 μm confocal stack with live cells stained green and dead cells stained red. The first is a representative image of a gel left in the dark and stained on day 1 after encapsulation (93 ± 3% live). The second is a representative image of a gel exposed to 15 minutes of 365 nm light at ~10 mW/cm^2 on day 1 after encapsulation and stained 1 hour later (90 ± 4% live). The third is a representative image of a gel exposed to 15 minutes of 365 nm light at ~10 mW/cm^2 on day 1 after encapsulation and stained 1 day later (90 ± 4% live).

Fig. 4 Schematic illustration of the three conditions that epithelial cells experience during the cyst-forming procedure, cross-sectional view. (i) First, cells form integrin binding sites with the CRGDS peptide in the microsphere network. (ii) Then, pre-cysts are encapsulated within the thiol-ene gel and cells form attachments to the CRGDS in the encapsulating gel. (iii) Finally, microspheres are eroded with light and with fast integrin turnover on the apical side only the integrins on the outside of the cyst retain their connections to the gel network.

Fig. 5 A549 cysts. (A) Bright field images of A549 cells progressively covering fibronectin-loaded microspheres. (B) Cross-section schematic illustrating the hollow cyst that remains in the hydrogel after erosion of the microsphere template. (C) Bright field image of an encapsulated A549 cyst after template erosion. (D) Maximum intensity projection of a confocal image stack of an A549 cyst, fixed 3 days after template erosion. Red is actin; blue is the cell nucleus. (E) Single confocal image through the center of the same A549 cyst demonstrating the hollow interior. Red is actin; blue is the cell nucleus.

Fig. 6 Primary cysts. (A) Bright field images of primary cells proliferating to cover the microspheres. (B) Bright field image of an encapsulated primary cell cyst after template erosion. (C) Maximum intensity projection of a confocal image stack of a primary cell cyst, fixed 3 days after template erosion. Green is T1α, a marker of the ATI cell phenotype; blue is the cell nucleus. (D) Single confocal image through the center of the same primary cell cyst demonstrating the hollow interior. Green is T1α, a marker of ATI cell phenotype; blue is the cell nucleus. (E) Maximum intensity projections of three 50 μm cryosections, documenting the absence of cells in the central lumen. Red is SPC, a marker of the ATII cell phenotype; green is T1α, a marker of the ATI cell phenotype; blue is the cell nucleus.

Fig. 7 Immunostaining of Primary Cysts. (A) Maximum intensity projections of a confocal image stack of a primary cell cyst, fixed 3 days after template erosion. Green is β-catenin, a marker of adherens junctions; red is ZO-1, a marker of tight junctions; blue is the cell nucleus. (B) Single confocal image through the center of the same primary cell cyst. Colors are the same as in A. (C) Maximum intensity projections of a confocal image stack of a primary cell cyst, fixed 6 days after template erosion. Green is T1α, a marker of the ATI cell phenotype; red is SPC, a marker of the ATII cell phenotype; blue is the cell nucleus. (D) Single confocal image through the center of the same primary cell cyst. Colors are the same as in C. (E) 3D surface projection of a 50 μm mouse lung tissue section showing multiple cysts, with on average 2 ATII cells per cyst. Colors are the same as in C.

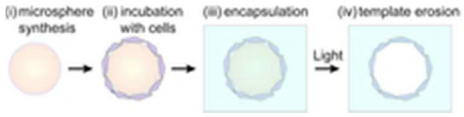

Fig. 1 Schematic of the overall cyst-forming procedure, cross-sectional view. (i) Bioadhesive, photodegradable microspheres (orange) were (ii) incubated with epithelial cells (purple) to coat the surface of the microspheres with cells. The cell-microsphere pre-cyst structures were (iii) encapsulated in a second bioadhesive hydrogel (blue), followed by (iv) erosion of the microsphere template with 365 nm light, leaving a hollow epithelial cyst inside the encapsulating hydrogel.
19x4mm (300 x 300 DPI)

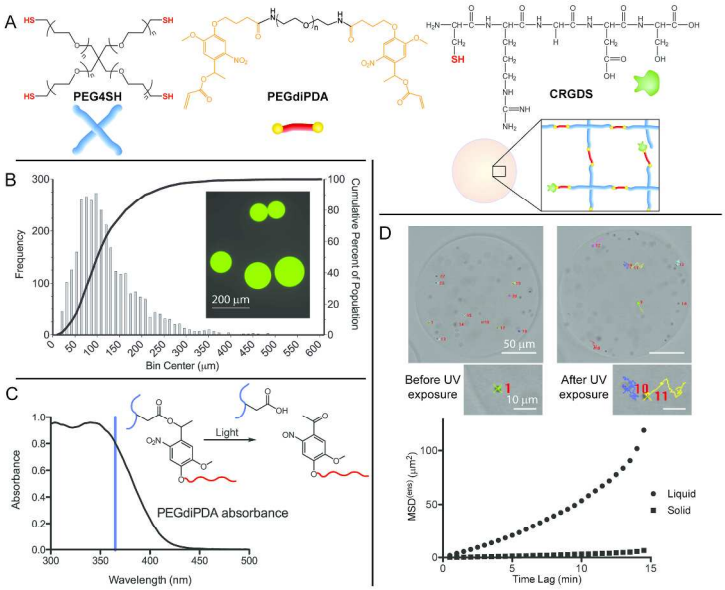

Fig. 2 Microsphere synthesis and erosion. (A) The microsphere hydrogel network was composed of poly(ethylene glycol) tetrathiol (PEG4SH; Mn ~5 kDa) and poly(ethylene glycol) di-photodegradable acrylate (PEGdiPDA; Mn ~4.1 kDa), with the bioadhesive peptide CRGDS included at 1.5 mM. The monomers were reacted via an inverse suspension polymerization using a base-catalyzed Michael addition to form the microspheres. (B) Microspheres labeled with a green fluorescent dye were imaged and analyzed to determine the size distribution. Histogram shows distribution of microsphere diameters, and the black line indicates the cumulative percentage of the population. Inset shows representative fluorescent image of microspheres used for diameter measurement. n = 3087 (C) The chemical structure indicates the cleavage of the nitrobenzyl ether moiety with light. The absorbance spectrum is for the PEGdiPDA crosslinker (0.8 mM) in phosphate-buffered saline, where the blue line indicates 365 nm. The molar extinction coefficient at 365 nm for the nitrobenzyl ether moiety was calculated to be ~5,000 L mol-1 cm-1. (D) Microspheres containing entrapped 2 μm diameter polystyrene beads were encapsulated in a second hydrogel and exposed to 365 nm light at an intensity of ~10 mW/cm2 for 15 minutes to erode the microspheres. Images

are of polystyrene bead tracks over 15 minutes before and after light exposure illustrating increased Brownian motion after microsphere erosion. The plot gives the ensemble mean squared displacement for the liquid and solid cases.
280x349mm (300 x 300 DPI)

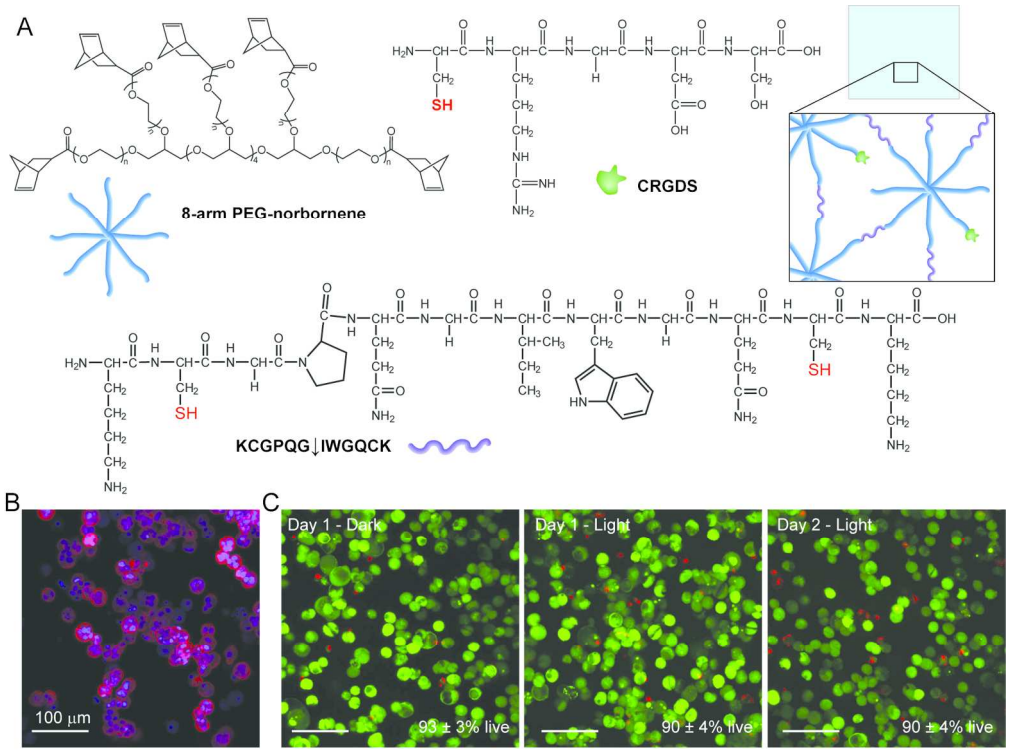

Fig. 3 Encapsulating hydrogel formulation. (A) The encapsulating gel was composed of 8-arm poly(ethylene glycol) functionalized with norbornene end groups (Mn ~40 kDa) and an enzymatically-cleavable di-cysteine peptide crosslinker (KCGPQG↓IWGQCK), with the adhesive peptide CRGDS included at 1 mM. The arrow indicates the enzymatic cleavage site. Thiol groups (red) react with the -ene functionalities on the 8-arm PEG through a radical-initiated thiol-ene polymerization. (B) Single cell suspension of A549 cells encapsulated in the thiol-ene gel. The image is a z-projection of a 250 µm confocal stack showing healthy actin cytoskeleton (red) and cell nuclei (blue). (C) Single cell suspension of A549 cells encapsulated in thiol-ene gels. The images are z-projections of a 500 µm confocal stack with live cells stained green and dead cells stained red. The first is a representative image of a gel left in the dark and stained on day 1 after encapsulation (93 ± 3% live). The second is a representative image of a gel exposed to 15 minutes of 365 nm light at ~10 mW/cm2 on day 1 after encapsulation and stained 1 hour later (90 ± 4% live). The third is a representative image of a gel exposed to 15 minutes of 365 nm light at ~10 mW/cm2 on day 1 after encapsulation and stained 1 day later (90 ± 4% live).
168x125mm (300 x 300 DPI)

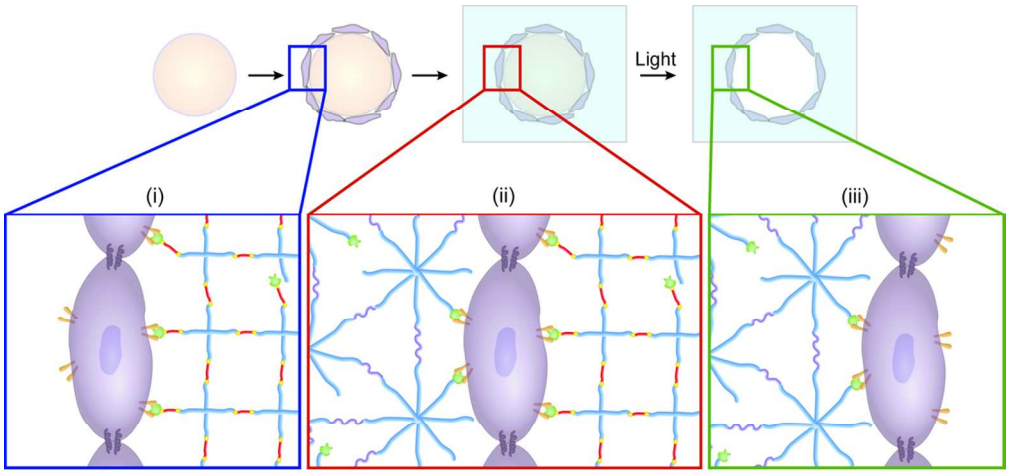

Fig. 4 Schematic illustration of the three conditions that epithelial cells experience during the cyst-forming procedure, cross-sectional view. (i) First, cells form integrin binding sites with the CRGDS peptide in the microsphere network. (ii) Then, pre-cysts are encapsulated within the thiol-ene gel and cells form attachments to the CRGDS in the encapsulating gel. (iii) Finally, microspheres are eroded with light and with fast integrin turnover on the apical side only the integrins on the outside of the cyst retain their connections to the gel network.
107x66mm (300 x 300 DPI)

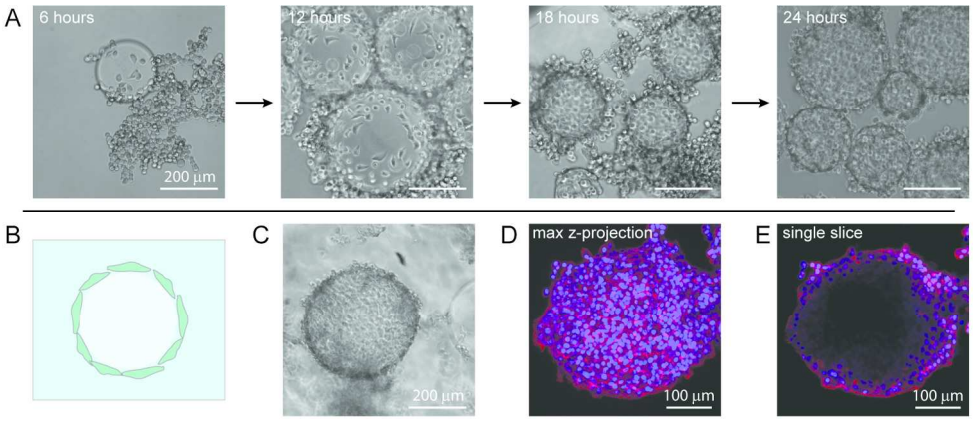

Fig. 5 A549 cysts. (A) Bright field images of A549 cells progressively covering fibronectin-loaded microspheres. (B) Cross-section schematic illustrating the hollow cyst that remains in the hydrogel after erosion of the microsphere template. (C) Bright field image of an encapsulated A549 cyst after template erosion. (D) Maximum intensity projection of a confocal image stack of an A549 cyst, fixed 3 days after template erosion. Red is actin; blue is the cell nucleus. (E) Single confocal image through the center of the same A549 cyst demonstrating the hollow interior. Red is actin; blue is the cell nucleus.
172x71mm (300 x 300 DPI)

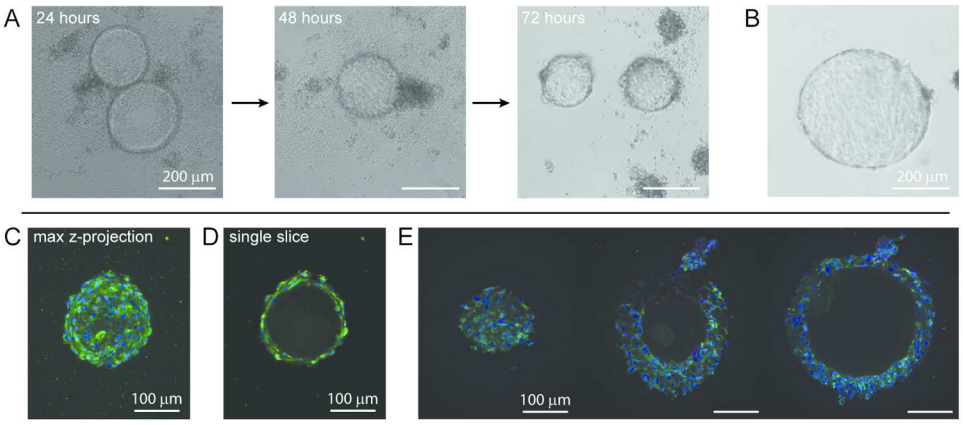

Fig. 6 Primary cysts. (A) Bright field images of primary cells proliferating to cover the microspheres. (B) Bright field image of an encapsulated primary cell cyst after template erosion. (C) Maximum intensity projection of a confocal image stack of a primary cell cyst, fixed 3 days after template erosion. Green is T1α, a marker of the ATI cell phenotype; blue is the cell nucleus. (D) Single confocal image through the center of the same primary cell cyst demonstrating the hollow interior. Green is T1α, a marker of ATI cell phenotype; blue is the cell nucleus. (E) Maximum intensity projections of three 50 μm cryosections, documenting the absence of cells in the central lumen. Red is SPC, a marker of the ATII cell phenotype; green is T1α, a marker of the ATI cell phenotype; blue is the cell nucleus.
172x71mm (300 x 300 DPI)

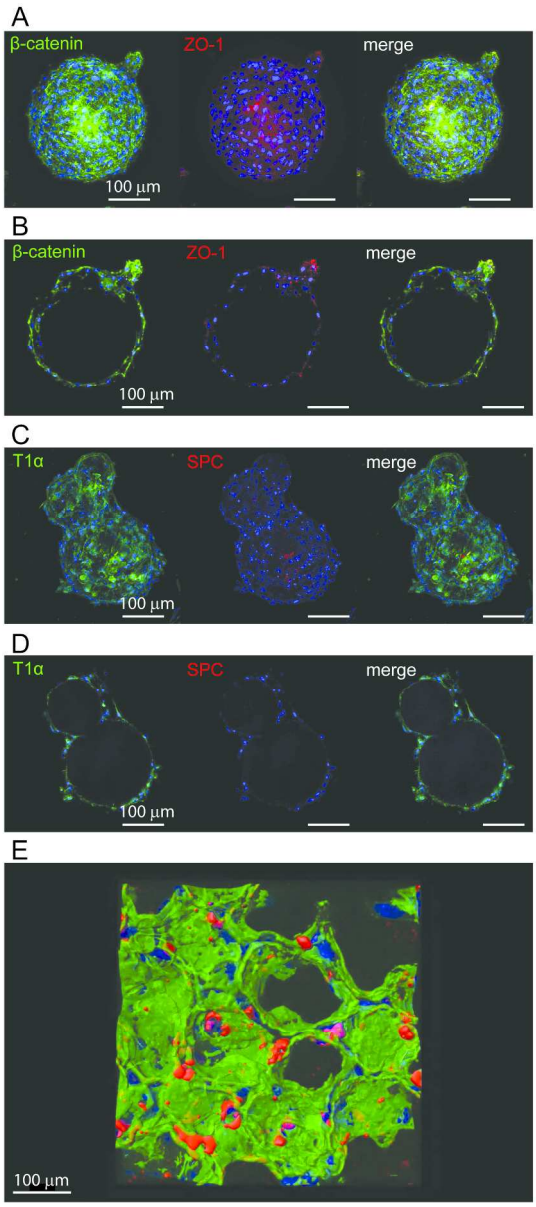

Fig. 7 Immunostaining of Primary Cysts. (A) Maximum intensity projections of a confocal image stack of a primary cell cyst, fixed 3 days after template erosion. Green is β-catenin, a marker of adherens junctions; red is ZO-1, a marker of tight junctions; blue is the cell nucleus. (B) Single confocal image through the center of the same primary cell cyst. Colors are the same as in A. (C) Maximum intensity projections of a confocal image stack of a primary cell cyst, fixed 6 days after template erosion. Green is T1α, a marker of the ATI cell phenotype; red is SPC, a marker of the ATII cell phenotype; blue is the cell nucleus. (D) Single confocal image through the center of the same primary cell cyst. Colors are the same as in C. (E) 3D surface projection of a 50 μm mouse lung tissue section showing multiple cysts, with on average 2 ATII cells per cyst. Colors are the same as in C.
190x395mm (300 x 300 DPI)